Metal–Organic Frameworks Hot Paper

How to cite:
International Edition: doi.org/10.1002/anie.202015359
German Edition: doi.org/10.1002/ange.202015359

Spectroscopic Evidence of Hyponitrite Radical Intermediate in NO Disproportionation at a MOF-Supported Mononuclear Copper Site

*Chenyue Sun, Luming Yang, Manuel A. Ortuño, Ashley M. Wright, Tianyang Chen, Ashley R. Head, Núria López, and Mircea Dincă**

Abstract: *Dianionic hyponitrite ($N_2O_2^{2-}$) is often proposed, based on model complexes, as the key intermediate in reductive coupling of nitric oxide to nitrous oxide at the bimetallic active sites of heme-copper oxidases and nitric oxide reductases. In this work, we examine the gas-solid reaction of nitric oxide with the metal–organic framework Cu^{I}-ZrTpmC* with a suite of in situ spectroscopies and density functional theory simulations, and identify an unusual chelating $N_2O_2^{\bullet-}$ intermediate. These results highlight the advantage provided by site-isolation in metal–organic frameworks (MOFs) for studying important reaction intermediates, and provide a mechanistic scenario compatible with the proposed one-electron couple in these enzymes.*

Introduction

The majority of naturally occurring nitrous oxide (N_2O) is produced by reductive homocoupling of nitric oxide (NO), $2\,NO + 2\,e^- + 2\,H^+ \rightarrow N_2O + H_2O$, catalyzed by various nitric oxide reductases (NORs) or heme-copper oxidases (HCOs).[1–3] The orchestrated cleavage and formation of strong N=O and N=N bonds are mediated by sophisticated binuclear centers, such as Fe(heme)-Fe(His)$_3$(Glu) in cNOR,[4] or Fe(heme)-Cu(His)$_3$ in HCO (Figure 1 a).[5] Mechanistically, it is widely acknowledged that the N=N bond forms with influx of two electrons to give a hyponitrite ($ON{=}NO^{2-}$) intermediate.[6] However, we know little about the temporal order of electron transfer steps versus N–N coupling.[7] Intriguingly, there are clues in favor of N–N coupling occurring at a $1\,e^-$-reduced bimetallic center, implying the formation of *monoanionic*, radical $N_2O_2^{\bullet-}$. One such clue is that the $2\,e^-$-reduced state is energetically highly unfavorable. Indeed, many studies find the heme in the bimetallic active site lying more than 200 mV below the standard reduction potential of the electron relay hemes and the non-heme metals (Fe_B or Cu_B).[8–11] In the case of Cu_B, this would entail a transformation from {CuNO}^{11} to a radical monoanionic hyponitrite, Cu^{II}-$N_2O_2^{\bullet-}$. To our knowledge, such an intermediate has not been observed yet, presumably due to its reactivity.

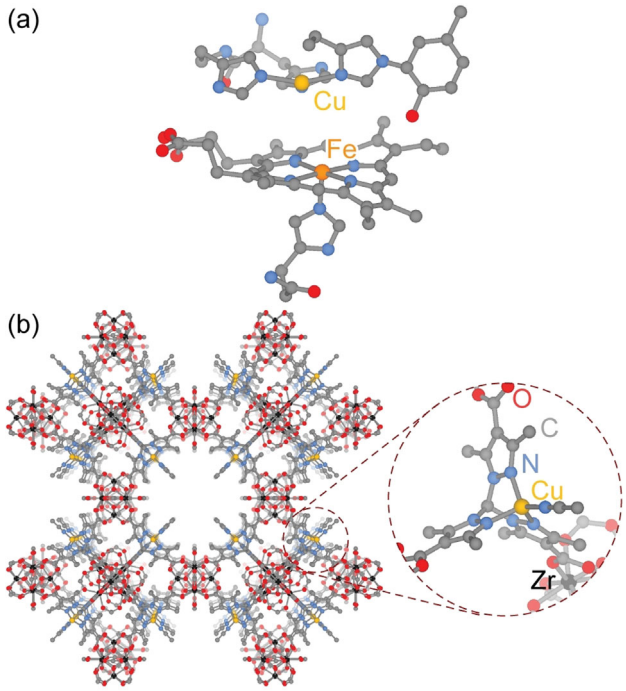

Figure 1. a) The bimetallic active site in cbb$_3$ oxidase, the most active NO-reducing HCO (PDB 3MK7). b) Structure of Cu^{I}-ZrTpmC* (**A**) and close-up at the metalloligand. An ideal full metalation is shown for simplicity. Hydrogen atoms and tetrafluoroborate anions are omitted for clarity. (Structure reported in Ref. [30].)

Molecular model systems often provide a fertile ground for understanding aspects of enzymatic mechanisms. In this case, much effort has been made to characterize the M-N_2O_2 unit in a biomimetic system.[12,13] In cases where M-N_2O_2 adducts are sufficiently stable to allow isolation and crystallographic characterization, exclusively dianionic $N_2O_2^{2-}$ species have been found (M = Cu,[14–16] Fe,[17] Co,[18] Ni,[19,20] or Pt[21]). However, caution should be taken to not conflate crystallized products with true intermediates.[18] The latter are arguably more directly identifiable through in situ spectroscopic methods. For this purpose, the stoichiometric disproportio-

[*] C. Sun, L. Yang, Dr. A. M. Wright, T. Chen, Prof. M. Dincă
Department of Chemistry, Massachusetts Institute of Technology
77 Massachusetts Avenue, Cambridge, MA 02139 (USA)
E-mail: mdinca@mit.edu
Dr. M. A. Ortuño, Prof. Dr. N. López
Institute of Chemical Research of Catalonia, The Barcelona Institute of Science and Technology
Av. Països Catalans 16, 43007 Tarragona (Spain)
Dr. A. R. Head
Center for Functional Nanomaterials, Brookhaven National Laboratory
Upton, NY 11973 (USA)
Supporting information and the ORCID identification number(s) for the author(s) of this article can be found under: https://doi.org/10.1002/anie.202015359.

nation of NO ($M^{n+} + 3NO \rightarrow M^{(n+1)+}\text{-}NO_2 + N_2O$) is often used as a surrogate reaction to reductive NO coupling, because formation of N_2O via disproportionation must also involve an $[N_2O_2]$ intermediate.[22–25] Earlier studies provided us with kinetic and, more recently, reactivity evidence that point to a monometallic $1e^-$-couple, suggestive of mono-anionic hyponitrite.[26–28] Herein we report comprehensive spectroscopic evidence of an isolable, mononuclear Cu^{II}-$N_2O_2^{\bullet-}$ intermediate, in the reaction between a MOF, Cu^{I}-ZrTpmC*, (**A**, Figure 1b) and NO.

Results and Discussion

We previously reported the synthesis of a ZrTpmC* MOF (Figure 1), wherein a NNN C_3-symmetric Tpm* metalloligand supports a tetrahedral Cu^I center capped by an acetonitrile molecule (Scheme 1, **A**). The copper sites lie at the triangular faces of interconnected cuboctahedral cavities with open

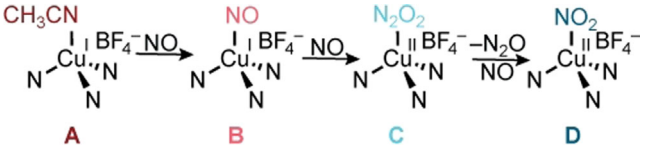

Scheme 1. Evolution of the copper site in Cu^I-ZrTpmC* under a flow of dilute NO.

metal sites pointing into the channel of the MOF. Schneider et al. showed that electron-poor Cu^I trispyrazolylborate (CuTp) analogues exhibit slow and unsynchronized Cu^{II}-NO_2 formation and Cu^I depletion, suggesting the presence of a long-lived intermediate.[29] Intrigued by these reports, we sought to identify such an intermediate by taking advantage of site-isolation of the similar Cu^I in **A**. Indeed, the ligand field of ZrTpmC* is similar to that of the electron deficient Tp^{CF_3,CH_3}, based on comparisons of ν(C-O) in LCu(I)-CO complexes (2110 cm^{-1} vs. 2109 cm^{-1}, respectively).[29,30] In addition, the neutral NNN environment in **A** is similar to the His_3 environment of Cu_B in various HCOs. **A** therefore approximates the coordination environment of the enzymatic Cu_B center.

To test the NO disproportionation activity of **A**, we performed diffuse-reflectance infrared Fourier-transform spectroscopy (DRIFTS) under a dilute stream of NO (25–500 ppm) in Ar at room temperature. The spectral changes can be divided into three stages (Figure 2; Figure S2 for ^{15}N-labeled DRIFTS). Immediately upon introduction of NO to **A** (Scheme 1), a band grows at 1757 cm^{-1} (**B**). This band shifts to 1728 cm^{-1} when ^{15}NO is used (calc. 1725 cm^{-1}) and is consistent with the N–O stretch of {CuNO}[11]. This value is considerably higher than that observed for the electron-rich $Tp^{R,R'}Cu(NO)$ (1710–1720 cm^{-1}) but is similar to that for the electron-poor $Tp^{CF_3,CH_3}Cu(NO)$ (1753 cm^{-1})[29] and cationic $[Tpm^{tBu,iPr}Cu(NO)]^+$ (1742 cm^{-1}).[31] The relatively high ν(N-O) is indicative of the weak $d_\pi(Cu)$-π*(NO) interaction and suggests that electron distribution in **B** can be regarded as largely pertaining to formal Cu^I and a neutral NO•, similar to

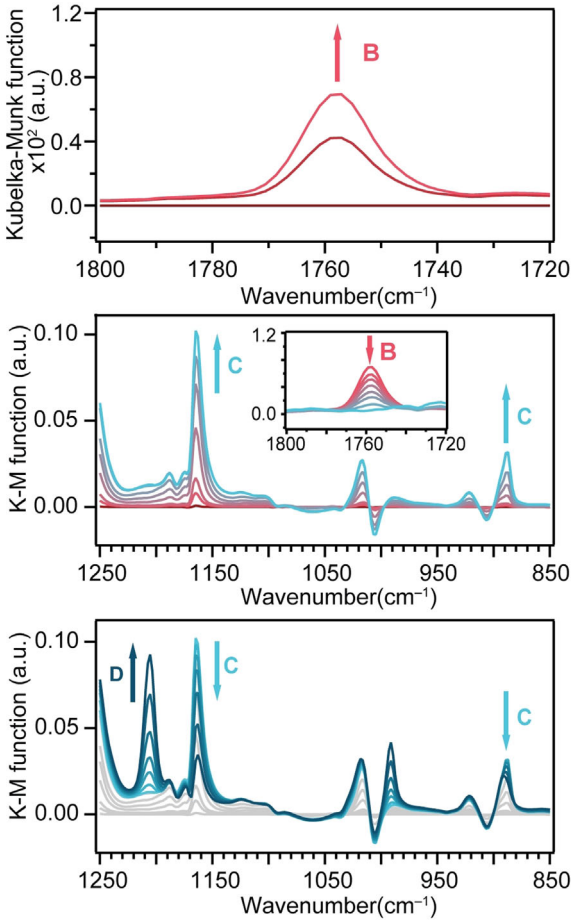

Figure 2. DRIFTS evolution of **A** under a flow of NO in argon, showing sequential formation of **B** (top), **C** (middle), and **D** (bottom). Changes over full spectral range can be found in the Supporting Information.

the related Tp complexes.[32] Under the dilute NO flow, the 1757 cm^{-1} band quickly diminishes and the second stage is dominated by the gradual growth of a second set of bands (species **C**). Isotope sensitive bands are found at 1163 cm^{-1} (^{15}N: 1148 cm^{-1}, calc. 1142 cm^{-1}) and 887 cm^{-1} (^{15}N: 883 cm^{-1}). These values are similar to those of $N_2O_2^{\bullet-}$ in Fe-MOF-5.[33] We accordingly assign **C** as a hyponitrite radical anion bound to Cu^{II}. Based on its associated isotope shift, the band at 1163 cm^{-1} can be assigned to one of the ν(N-O); assignment of the second band required computation (vide infra). No other isotope-sensitive bands could be discerned but we note that the complex spectral changes associated with framework vibrations may well conceal any less prominent NO-related features. In the final stage, bands associated with **C** decline and the spectrum evolves along with the emergence of a new species **D**. The transformation of **C** to **D** is clearly dependent on NO: in the absence of NO, no features of **D** can be observed, and the rate of formation of **D** is clearly correlated to [NO]. Only one isotope-sensitive band at 1205 cm^{-1} (^{15}N 1180 cm^{-1}, calc. 1183 cm^{-1}) can be confidently assigned as ν_{as}(N-O) in Cu^{II}-nitrito,[34] with the corresponding ν_s and δ modes likely obscured by framework vibrational modes. Detailed assignment of the IR features is discussed in

the computational section. Additional evidence supporting Scheme 1 can be found in the SI.

Although **B** is only transiently formed under NO flow, it is the predominant species when NO is substoichiometric. This enables isolation of **B** and further in situ characterization. Diffuse-reflectance UV-visible-NIR spectroscopy (DRUVS, Figure S3 and S3) uncovers an electronic transition as a shoulder at 450 nm which can be assigned as a Cu→NO charge transfer (CT) band.[31] With an excitation wavelength of 473 nm, resonance-enhanced Raman bands at 1762 cm^{-1} (^{15}N: 1731 cm^{-1}) and 434 cm^{-1} (^{15}N: 429 cm^{-1}) can be found for **B**, which correspond to ν(N-O) and ν(Cu-NO) (Figure S4). An electron paramagnetic resonance (EPR) spectrum of **B** measured at 4.4 K displays a reverse-axial pattern ($g_{\|} < g_{\perp}$) of an $S = 1/2$ spin, with hyperfine coupling to both copper ($I_{Cu} = 3/2$) and nitrogen ($I_N = 1$) (Figure 4). This spectrum can be simulated well with $g_{\|} = 1.81$, $g_{\perp} = 1.98$, $A_{Cu_{\|}} = 143$ G, $A_{Cu_{\perp}} = 110$ G, and $A_{N_{\|}} = 30$ G (Figure S5), where the small g-values and large $A_{N_{\|}}$ point to significant spin density population on the nitrogen atom in the nitrosyl ligand. All of these observations agree well with the EPR pattern for a typical Cu^{I}-nitrosyl compound.[32]

Species **C** is also sufficiently stable to allow inspection by additional spectroscopic techniques. DRUVS (Figure 3) of the greenish yellow **C** under nitrogen revealed ligand-field (LF) transitions at 745 and 1065 nm, as well as charge transfer bands at 315 and 395 nm. The LF bands are clearly indicative of Cu^{II}. The band at 395 nm recedes when **C** converts to **D** (Figure S3), leading us to tentatively assign it as a Cu→$N_2O_2^{\bullet-}$ CT band. In contrast, the blue-green **D** shows LF bands at 700 and 950 nm and CT band at 300 nm. An X-band EPR spectrum of **C** measured at 4.4 K shows an axial signal typical for a spin coupled to copper, with $g_{\|} = 2.30$, $g_{\perp} = 2.06$, $A_{Cu_{\|}} =$ 170 G, and $A_{Cu_{\perp}} = 20$ G (Figure S4, Figure S5). X-ray photoelectron spectroscopy (XPS) data of **C** exhibited a N1s peak 0.8 eV higher than those pertaining to the pyrazole nitrogen signals, which can be assigned to $N_2O_2^{\bullet-}$ (Figure S7).

The key evidence in support of assigning **C** as a two-spin system came from parallel mode EPR measurements, where the relative intensity of the $\Delta m_s = \pm 2$ transitions is enhanced. At 4.4 K, **C** exhibits a transition at 1688 G ($g = 3.96$) that is absent in the perpendicular mode spectrum (Figure S5). This agrees well with the expected transition at half-field typical for a triplet system arising from the coupling between the Cu^{II} and nitrogen-centered spins.[35] To validate this assignment, we performed variable-temperature EPR in the range of 4.4–55 K in perpendicular mode, which has better signal-to-noise ratio (Figure 4b). For a spin exchange-coupled system, the nature of the coupling can be deciphered by comparing the temperature dependence of the signal intensity with the Curie law.[36] For **C**, as the temperature increases, both the peak amplitude and the integrated intensity of the signal of interest

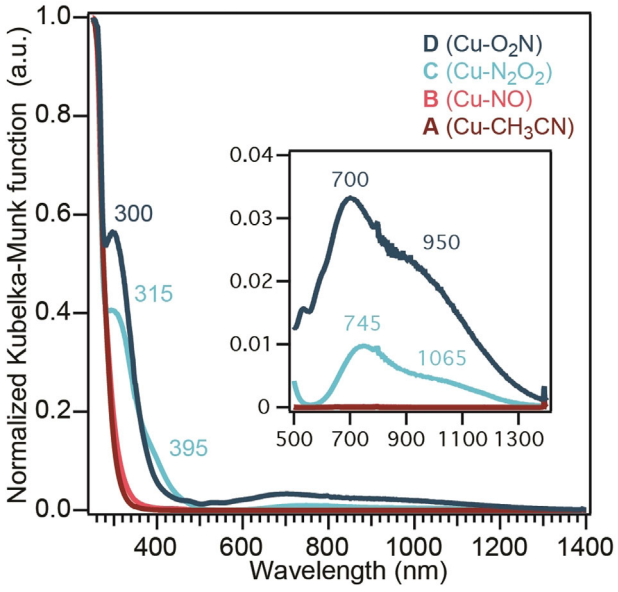

Figure 3. Diffuse-reflectance UV-vis-NIR at different stages of NO reaction. λ_{max} at 395 nm is tentatively assigned to CT in Cu^{II}-$N_2O_2^{\bullet-}$.

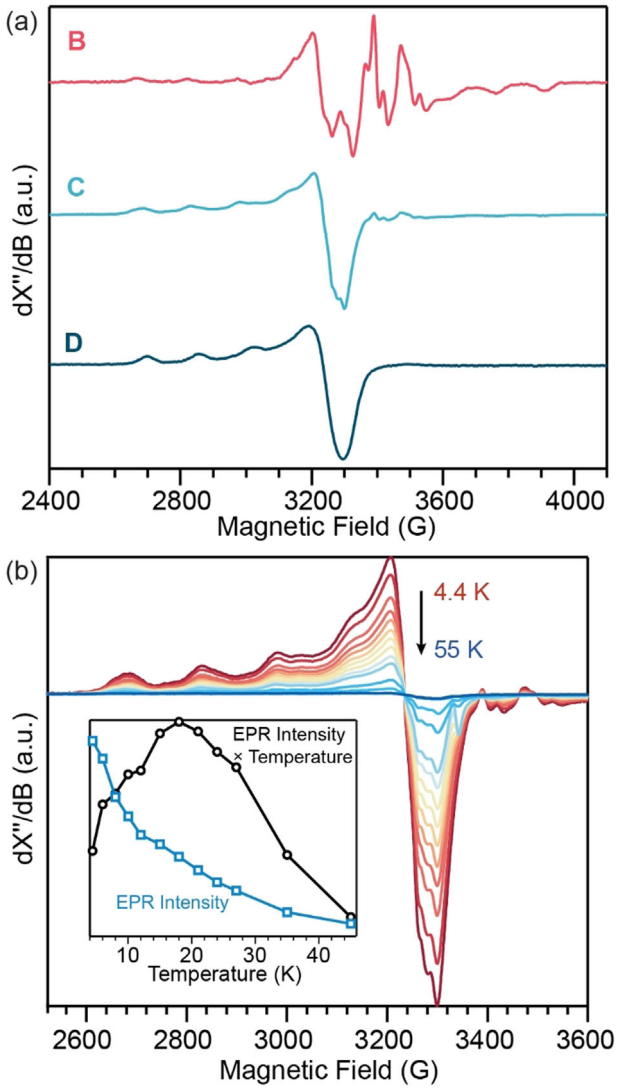

Figure 4. a) X-band EPR spectra for **B**, **C**, and **D** measured at 4.4 K under perpendicular mode. b) Variable temperature EPR spectra of **C** from 4.4 to 55 K. Inset shows the temperature dependence of double-integrated EPR intensity and the product of double integral and temperature.

decrease while preserving the line shape and linewidth (Figure S6). A closer look at the product of temperature and double-integrated EPR intensity reveals that this value increases to a maximum near 20 K before decreasing at higher temperatures (Figure 4b inset). This temperature dependence agrees well with the expected behavior for two ferromagnetically coupled spins with zero-field splitting, while thermal broadening is discounted based on invariance of the spectral linewidth.[37,38]

The Cu^{II}-nitrite product **D** does not react further with NO under our reaction conditions. X-band EPR of **D** at 5 K displays a typical Cu^{II} signal with axial symmetry ($g_{\parallel}=2.25$, $g_{\perp}=2.04$) (Figure S6). The large $A_{Cu_{\parallel}}=165$ G points to localization of the spin density on Cu^{II}. The absence of notable hyperfine coupling to nitrogen agrees with the assignment of a κ^2 oxygen-bound Cu^{II}-nitrito species. Importantly, powder X-ray diffraction (PXRD) of **D** shows retention of crystallinity (Figure S8), confirming that the structural integrity of the MOF itself is preserved.

A variety of linkage isomers for hyponitrite and nitrite are commonly seen in the literature.[13,39] To further corroborate our spectroscopic studies and assignments in this context, we turned to density functional theory (DFT) simulations.[40] The unit cell of ZrTpmC* was optimized at the PBE-D3 level and a cluster model containing the core $[Cu^{I}\text{-TpmC*}]^{+}[BF_4]^{-}$ was computed at the B3LYP-D3 level of theory, fixing the coordinates of the carboxylate C atoms to mimic the framework rigidity. The use of hybrid density functionals is recommended to properly account for different Cu oxidation states.[41] Full details can be found in the SI and the ioChem-BD repository.[42]

The most stable computed structures for **B**, **C**, and **D** are shown in Figure 5 (see Figure S11 for other isomers and spin states). It is found that TpmC* becomes κ^2 in **B**, **C**, and **D** (Cu-N ≈ 2.0 Å, Cu···N 2.5–2.6 Å) and the BF_4^- therein interacts rather strongly with Cu (Cu···F ≈ 2.3 Å). Strong interactions between Cu and BF_4^- are precedented.[43] The calculated spin density (ρ) is consistent with our assignment from EPR and electronic spectroscopy. Species **B** is a doublet with a Cu^{I} center ($\rho=0.0$) and a (κN)-$NO^{\bullet}$ ligand ($\rho=1.0$). Species **C** is a triplet with a Cu^{II} center ($\rho=0.7$) and a *cis*-($\kappa O,\kappa O'$)-$N_2O_2^{\bullet-}$ ligand ($\rho=1.2$) (Figure S12). The open-shell singlet has a similar energy (3.6 kJ mol^{-1} above triplet **C**), while the closed-shell singlet (Cu^{3+}-$N_2O_2^{2-}$) is significantly less stable (33.3 kJ mol^{-1} above triplet **C**). The energy difference between the open-shell singlet and triplet is slightly functional-dependent but the order is invariant (Figure S13). Lastly, species **D** is a doublet with a Cu^{II} center ($\rho=0.7$) and a ($\kappa O,\kappa O'$)-NO_2^- ligand ($\rho=0.2$), all in good agreement with our spectroscopic assignments.

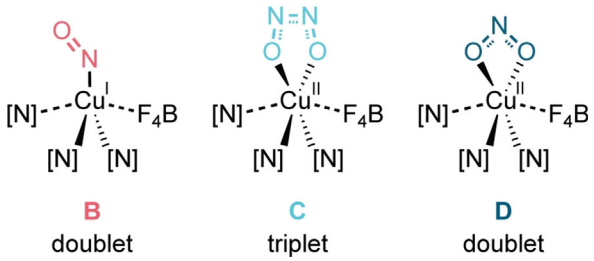

Figure 5. DFT-optimized structures and lowest-energy spin states for **B**, **C**, and **D**.

The computed vibrational frequencies for **B**–**D** are shown in Table 1. They are also in line with the experimental values. Calculations for **B** give ν(N-O) at 1766 cm^{-1} (exp. IR 1757 cm^{-1}, rR 1762 cm^{-1}). Omitting BF_4^- yields a larger value of 1812 cm^{-1}, further supporting a Cu-BF_4 interaction. ν(Cu-NO) is found at 410 cm^{-1} (exp. 434 cm^{-1}). Two main bands are computed for the N_2O_2 moiety in **C** in the region 1300-600 cm^{-1}: ν_a(N-O) at 1183 cm^{-1} (exp. 1163 cm^{-1}) and $\delta_{sym.bend}$-(NNO) at 913 cm^{-1} (exp. 887 cm^{-1}). No vibrational modes in the region 1600-1300 cm^{-1} can be associated with the N_2O_2 group. The nitrito species in **D** computes with an asymmetric N-O stretch at 1201 cm^{-1} (exp. 1205 cm^{-1}). The computed ν_s(N-O) and δ(ONO) appear at 1308 cm^{-1} and 857 cm^{-1}, respectively. Finally, the isotope shifts in vibrational frequencies are also well reproduced.

Table 1: Computed vibrational frequencies (cm^{-1}).

Species	B	C[a]	D
^{14}N comp.	1766, 410	1183, 913	1201
^{14}N exp.[b]	1757	1163, 887	1205
^{14}N exp.[c]	1762, 434		
^{15}N comp.	1734, 403	1148, 895	1177
^{15}N exp.[b]	1728	1159, 883	1180
^{15}N exp.[c]	1731, 429		

[a] Calculated based on the triplet state of **C**. [b] Experimental values from DRIFTS. [c] Experimental values from resonance Raman.

Conclusion

In summary, detailed spectroscopic investigation of NO disproportionation with a Cu center within a MOF identifies the key intermediate of the N–N coupling step as a *cis*-($\kappa O,\kappa O'$)-$N_2O_2^{\bullet-}$ ligand bound to Cu^{II}. This unusual intermediate is isolable at room temperature owing to spatial isolation within a pore. These results contribute to mounting evidence for the utility of MOFs in the isolation of extremely reactive species that are difficult to investigate with other platforms.[44–50] This strategy is particularly effective in gas-solid systems and with weak ligands such as Tpm, which tend to demetalate in solution. Indeed, in our hands, passing NO through a solution of $[Cu(CH_3CN)BF_4]$TpmC*-Et (TpmC*-Et is the ethyl ester of TpmC*) in CH_2Cl_2 led to immediate formation of the homoleptic bis-Tpm complex and no observable intermediate. This strategy may be valuable for the study of intermediates of relevance to enzymatic catalysis. Here, although the Cu^{I}-ZrTpmC* is evidently not a faithful structural or functional mimic of the Cu_B site in HCO, it presents the conceptual framework for discussing the intermediacy of an $N_2O_2^{\bullet-}$ species at Cu_B in 1 e$^-$-reduced HCO, en route to $N_2O_2^{2-}$.

Acknowledgements

This research was funded by the National Science Foundation through the Alan T. Waterman Award to M.D. (DMR-1645232). This research used resources of the Center for Functional Nanomaterials, which is a U.S. DOE Office of Science Facility, at Brookhaven National Laboratory under Contract No. DE-SC0012704. M.A.O. acknowledges the support of the Beatriu de Pinós postdoctoral program of the Government of Catalonia's Secretariat for Universities and Research of the Ministry of Economy and Knowledge (2017-BP-00039).

Conflict of interest

The authors declare no conflict of interest.

Keywords: bioinorganic chemistry · metal–organic frameworks (MOFs) · nitrogen oxides

[1] J. Hendriks, A. Oubrie, J. Castresana, A. Urbani, S. Gemeinhardt, M. Saraste, *Biochim. Biophys. Acta Bioenerg.* **2000**, *1459*, 266 – 273.
[2] A. Giuffrè, G. Stubauer, P. Sarti, M. Brunori, W. G. Zumft, G. Buse, T. Soulimane, *Proc. Natl. Acad. Sci. USA* **1999**, *96*, 14718 – 14723.
[3] E. Forte, A. Urbani, M. Saraste, P. Sarti, M. Brunori, A. Giuffrè, *Eur. J. Biochem.* **2001**, *268*, 6486 – 6491.
[4] T. Hino, Y. Matsumoto, S. Nagano, H. Sugimoto, Y. Fukumori, T. Murata, S. Iwata, Y. Shiro, *Science* **2010**, *330*, 1666 – 1670.
[5] L. M. Hunsicker-Wang, R. L. Pacoma, Y. Chen, J. A. Fee, C. D. Stout, *Acta Crystallogr. Sect. D* **2005**, *61*, 340 – 343.
[6] C. Varotsis, T. Ohta, T. Kitagawa, T. Soulimane, E. Pinakoulaki, *Angew. Chem. Int. Ed.* **2007**, *46*, 2210 – 2214; *Angew. Chem.* **2007**, *119*, 2260 – 2264.
[7] C. Ferousi, S. H. Majer, I. M. DiMucci, K. M. Lancaster, *Chem. Rev.* **2020**, *120*, 5252 – 5307.
[8] K. L. C. Grönberg, M. D. Roldán, L. Prior, G. Butland, M. R. Cheesman, D. J. Richardson, S. Spiro, A. J. Thomson, N. J. Watmough, *Biochemistry* **1999**, *38*, 13780 – 13786.
[9] V. Rauhamäki, D. A. Bloch, M. I. Verkhovsky, M. Wikström, *J. Biol. Chem.* **2009**, *284*, 11301 – 11308.
[10] F. Melin, H. Xie, T. Meyer, Y. O. Ahn, R. B. Gennis, H. Michel, P. Hellwig, *Biochim. Biophys. Acta Bioenerg.* **2016**, *1857*, 1892 – 1899.
[11] M. Kato, S. Nakagawa, T. Tosha, Y. Shiro, Y. Masuda, K. Nakata, I. Yagi, *J. Phys. Chem. Lett.* **2018**, *9*, 5196 – 5200.
[12] M. P. Schopfer, J. Wang, K. D. Karlin, *Inorg. Chem.* **2010**, *49*, 6267 – 6282.
[13] A. M. Wright, T. W. Hayton, *Inorg. Chem.* **2015**, *54*, 9330 – 9341.
[14] G. B. Wijeratne, S. Hematian, M. A. Siegler, K. D. Karlin, *J. Am. Chem. Soc.* **2017**, *139*, 13276 – 13279.
[15] D. Lionetti, G. De Ruiter, T. Agapie, *J. Am. Chem. Soc.* **2016**, *138*, 5008 – 5011.
[16] G. B. Wijeratne, M. Bhadra, M. A. Siegler, K. D. Karlin, *J. Am. Chem. Soc.* **2019**, *141*, 17962 – 17967.
[17] N. Xu, A. L. O. Campbell, D. R. Powell, J. Khandogin, G. B. Richter-Addo, *J. Am. Chem. Soc.* **2009**, *131*, 2460 – 2461.
[18] B. F. Hoskins, F. D. Whillans, D. H. Dale, D. C. Hodgkin, *J. Chem. Soc. D* **1969**, 69.
[19] A. M. Wright, G. Wu, T. W. Hayton, *J. Am. Chem. Soc.* **2012**, *134*, 9930 – 9933.
[20] S. Kundu, P. N. Phu, P. Ghosh, S. A. Kozimor, J. A. Bertke, S. C. E. Stieber, T. H. Warren, *J. Am. Chem. Soc.* **2019**, *141*, 1415 – 1419.
[21] N. Arulsamy, D. S. Bohle, J. A. Imonigie, S. Levine, *Angew. Chem. Int. Ed.* **2002**, *41*, 2371 – 2373; *Angew. Chem.* **2002**, *114*, 2477 – 2479.
[22] K. J. Franz, S. J. Lippard, *J. Am. Chem. Soc.* **1998**, *120*, 9034 – 9040.
[23] G. G. Martirosyan, A. S. Azizyan, T. S. Kurtikyan, P. C. Ford, *Inorg. Chem.* **2006**, *45*, 4079 – 4087.
[24] J. P. Collman, Y. Yang, A. Dey, R. A. Decréau, S. Ghosh, T. Ohta, E. I. Solomon, *Proc. Natl. Acad. Sci. USA* **2008**, *105*, 15660 – 15665.
[25] J. Wang, M. P. Schopfer, S. C. Puiu, A. A. N. Sarjeant, K. D. Karlin, *Inorg. Chem.* **2010**, *49*, 1404 – 1419.
[26] C. E. Ruggiero, S. M. Carrier, W. B. Tolman, *Angew. Chem. Int. Ed. Engl.* **1994**, *33*, 895 – 897; *Angew. Chem.* **1994**, *106*, 917 – 919.
[27] E. G. Abucayon, R. L. Khade, D. R. Powell, Y. Zhang, G. B. Richter-Addo, *J. Am. Chem. Soc.* **2018**, *140*, 4204 – 4207.
[28] S. Sabuncu, J. H. Reed, Y. Lu, P. Moënne-Loccoz, *J. Am. Chem. Soc.* **2018**, *140*, 17389 – 17393.
[29] J. L. Schneider, S. M. Carrier, C. E. Ruggiero, V. G. Young, W. B. Tolman, *J. Am. Chem. Soc.* **1998**, *120*, 11408 – 11418.
[30] C. Sun, G. Skorupskii, J. H. Dou, A. M. Wright, M. Dincă, *J. Am. Chem. Soc.* **2018**, *140*, 17394 – 17398.
[31] K. Fujisawa, A. Tateda, Y. Miyashita, K. I. Okamoto, F. Paulat, V. K. K. Praneeth, A. Merkle, N. Lehnert, *J. Am. Chem. Soc.* **2008**, *130*, 1205 – 1213.
[32] C. E. Ruggiero, S. M. Carrier, W. E. Antholine, J. W. Whittaker, C. J. Cramer, W. B. Tolman, *J. Am. Chem. Soc.* **1993**, *115*, 11285 – 11298.
[33] C. K. Brozek, J. T. Miller, S. A. Stoian, M. Dincă, *J. Am. Chem. Soc.* **2015**, *137*, 7495 – 7501.
[34] N. Lehnert, U. Cornelissen, F. Neese, T. Ono, Y. Noguchi, K. I. Okamoto, K. Fujisawa, *Inorg. Chem.* **2007**, *46*, 3916 – 3933.
[35] S. S. Eaton, K. M. More, B. M. Sawant, G. R. Eaton, *J. Am. Chem. Soc.* **1983**, *105*, 6560 – 6567.
[36] A. Bencini, D. Gatteschi, *Electron Paramagnetic Resonance of Exchange Coupled Systems*, Springer Berlin Heidelberg, Berlin, **1990**.
[37] G. R. Eaton, S. S. Eaton, D. P. Barr, R. T. Weber, *Quantitative EPR*, Springer Vienna, Vienna, **2010**.
[38] W. R. Hagen, H. Wassink, R. R. Eady, B. E. Smith, H. Haaker, *Eur. J. Biochem.* **1987**, *169*, 457 – 465.
[39] S. Metz, *Inorg. Chem.* **2017**, *56*, 3820 – 3833.
[40] S. O. Odoh, C. J. Cramer, D. G. Truhlar, L. Gagliardi, *Chem. Rev.* **2015**, *115*, 6051 – 6111.
[41] B. Dereli, M. A. Ortuño, C. J. Cramer, *ChemPhysChem* **2018**, *19*, 959 – 966.
[42] a) M. Álvarez-Moreno, C. De Graaf, N. López, F. Maseras, J. M. Poblet, C. Bo, *J. Chem. Inf. Model.* **2015**, *55*, 95 – 103; b) M. A. Ortuño, 2021, ioChem-BD database, DOI: https://doi.org/10.19061/iochem-bd-1-160.
[43] A. Hazell, R. Hazell, C. J. McKenzie, L. P. Nielsen, *Dalton Trans.* **2003**, 2203 – 2208.
[44] E. D. Bloch, L. J. Murray, W. L. Queen, S. Chavan, S. N. Maximoff, J. P. Bigi, R. Krishna, V. K. Peterson, F. Grandjean, G. J. Long, B. Smit, S. Bordiga, C. M. Brown, J. R. Long, *J. Am. Chem. Soc.* **2011**, *133*, 14814 – 14822.
[45] D. J. Xiao, E. D. Bloch, J. A. Mason, W. L. Queen, M. R. Hudson, N. Planas, J. Borycz, A. L. Dzubak, P. Verma, K. Lee, F. Bonino, V. Crocellà, J. Yano, S. Bordiga, D. G. Truhlar, L. Gagliardi, C. M. Brown, J. R. Long, *Nat. Chem.* **2014**, *6*, 590 – 595.
[46] S. Øien, G. Agostini, S. Svelle, E. Borfecchia, K. A. Lomachenko, L. Mino, E. Gallo, S. Bordiga, U. Olsbye, K. P. Lillerud, C. Lamberti, *Chem. Mater.* **2015**, *27*, 1042 – 1056.

[47] T. Zhang, K. Manna, W. Lin, *J. Am. Chem. Soc.* **2016**, *138*, 3241 – 3249.
[48] A. Burgun, C. J. Coghlan, D. M. Huang, W. Chen, S. Horike, S. Kitagawa, J. F. Alvino, G. F. Metha, C. J. Sumby, C. J. Doonan, *Angew. Chem. Int. Ed.* **2017**, *56*, 8412 – 8416; *Angew. Chem.* **2017**, *129*, 8532 – 8536.
[49] A. M. Abdel-Mageed, B. Rungtaweevoranit, M. Parlinska-Wojtan, X. Pei, O. M. Yaghi, R. J. Behm, *J. Am. Chem. Soc.* **2019**, *141*, 5201 – 5210.
[50] A. Das, Y.-S. Chen, J. H. Reibenspies, D. C. Powers, *J. Am. Chem. Soc.* **2019**, *141*, 16232 – 16236.

Manuscript received: November 17, 2020
Version of record online: ■■ ■■, ■■■■

Research Articles

Metal–Organic Frameworks

C. Sun, L. Yang, M. A. Ortuño, A. M. Wright, T. Chen, A. R. Head, N. López, M. Dincă* ——— ■■■■–■■■■

Spectroscopic Evidence of Hyponitrite Radical Intermediate in NO Disproportionation at a MOF-Supported Mononuclear Copper Site

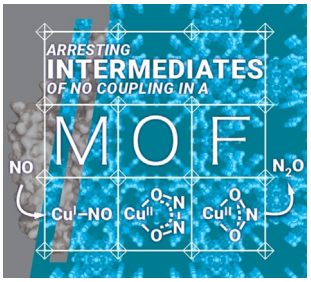

A radical $N_2O_2^{\bullet-}$ intermediate formed during a nitric oxide reductive coupling reaction was captured at a copper center in a metal–organic framework (MOF). Strict site isolation in the solid state is key in stabilizing this intermediate.